

## Reactions of 2-Methyltetrahydropyran on Silica Supported Nickel Phosphide, in Comparison with 2-Methyltetrahydrofuran

Phuong P. Bui, S. Ted Oyama, Atsushi Takagaki, Brad P. Carrow, and Kyoko Nozaki

ACS Catal., Just Accepted Manuscript • DOI: 10.1021/acscatal.6b01033 • Publication Date (Web): 01 Jun 2016

Downloaded from <http://pubs.acs.org> on June 7, 2016

### Just Accepted

“Just Accepted” manuscripts have been peer-reviewed and accepted for publication. They are posted online prior to technical editing, formatting for publication and author proofing. The American Chemical Society provides “Just Accepted” as a free service to the research community to expedite the dissemination of scientific material as soon as possible after acceptance. “Just Accepted” manuscripts appear in full in PDF format accompanied by an HTML abstract. “Just Accepted” manuscripts have been fully peer reviewed, but should not be considered the official version of record. They are accessible to all readers and citable by the Digital Object Identifier (DOI®). “Just Accepted” is an optional service offered to authors. Therefore, the “Just Accepted” Web site may not include all articles that will be published in the journal. After a manuscript is technically edited and formatted, it will be removed from the “Just Accepted” Web site and published as an ASAP article. Note that technical editing may introduce minor changes to the manuscript text and/or graphics which could affect content, and all legal disclaimers and ethical guidelines that apply to the journal pertain. ACS cannot be held responsible for errors or consequences arising from the use of information contained in these “Just Accepted” manuscripts.

1  
2  
3  
4  
5  
6  
7  
8  
9  
10 **Reactions of 2-Methyltetrahydropyran on Silica Supported Nickel Phosphide, in**  
11 **Comparison with 2-Methyltetrahydrofuran**  
12  
13  
14

15 Phuong P. Bui<sup>1,2</sup>, S. Ted Oyama<sup>1,2\*</sup>, Atsushi Takagaki<sup>1</sup>, Brad P. Carrow<sup>3,4</sup>, Kyoko Nozaki<sup>3</sup>  
16  
17

- 18  
19 1. The University of Tokyo, Department of Chemical Systems Engineering,  
20  
21 7-3-1 Hongo, Tokyo, 13-8656, Japan.  
22  
23 2. Virginia Tech, Department of Chemical Engineering, Blacksburg, VA, USA  
24  
25 3. The University of Tokyo, Department Department of Chemistry and Biotechnology,  
26  
27 7-3-1 Hongo, Tokyo, 13-8656, Japan..  
28  
29 4. Princeton University, Department of Chemistry, Princeton, NJ, USA.  
30  
31  
32  
33  
34  
35  
36  
37  
38  
39

40 Corresponding author email: oyama@vt.edu  
41  
42  
43  
44  
45  
46  
47  
48  
49  
50  
51  
52  
53  
54  
55  
56  
57  
58  
59  
60

## Abstract

The reactions of 2-methyltetrahydropyran (2-MTHP, C<sub>6</sub>H<sub>12</sub>O) on Ni<sub>2</sub>P/SiO<sub>2</sub> provide insights on the interactions between a cyclic ether, an abundant component of biomass feedstock, with a transition metal phosphide, an effective hydrotreating catalyst. At atmospheric pressure and a low contact time, conditions similar to those of a fast pyrolysis process, 70% of products formed from the reaction of 2-MTHP on Ni<sub>2</sub>P/SiO<sub>2</sub> were deoxygenated products, 2-hexene and 2-pentenes, indicating a good oxygen removal capacity. Deprotonation, hydrogenolysis, dehydration, and decarbonylation were the main reaction routes. The reaction sequence started with the adsorption of 2-MTHP, followed by ring-opening steps on either the methyl substituted side (Path I) or the unsubstituted side (Path II) to produce adsorbed alkoxide species. In Path I, a primary alkoxide was oxidized at the  $\alpha$ -carbon to produce an aldehyde which subsequently underwent decarbonylation to 2-pentenes. The primary alkoxide could also be protonated to give a primary alcohol which could desorb or form the final product 2-hexene. In Path II, a secondary alkoxide was oxidized to produce a ketone or was protonated to a secondary alcohol that was dehydrated to give 2-hexene. The active sites for the adsorption of 2-MTHP and *O*-intermediates were likely to be Ni sites.

**Keywords:** Hydrodeoxygenation; 2-methyltetrahydropyran; nickel phosphide; contact time studies; reaction network.

## 1. Introduction

Meeting the ever-growing demand for transportation fuels and chemical feedstocks is of significant worldwide importance. Among the various renewable energy types, like solar, wind, or wave, only bioresources satisfy both needs, and continuous efforts have been expended in developing biomass processing technology [1,2,3]. Data obtained from different sciences such as analytical chemistry [4,5], fundamental catalysis [6,7,8], and mathematical modelling [9,10,11] are used to improve the technology for biomass conversion. Our work contributes to understanding the interactions between a catalyst and a compound, 2-methyltetrahydropyran ( $C_6H_{12}O$ ), whose structure is close to those of components in the biomass resources. Specifically, many compounds derived from cellulose and hemicellulose have six-membered rings with internal ether linkages like the pyran ring.

A central issue of biomass and bio-oil treatments is the removal of large amounts of multifunctional oxygenate compounds as they decrease heating value and cause chemical and physical instability in the final fuel products [12]. The complex composition requires thorough research on how each component reacts on a catalyst, thus mechanistic studies on model compounds of these constituents provide valuable insights to this end. This study describes the reactions of 2-methyltetrahydropyran (2-MTHP) on silica-supported nickel phosphide. The reactant has a six-member ether ring with a methyl group attached to one alpha-carbon. Analogous compounds with five-member ether rings such as furan and furan derivatives were investigated on various catalysts including conventional hydrotreating catalysts [13-19], noble metals [20-31], metals [32-34], and metal phosphides [35-39].

1  
2  
3  
4  
5  
6  
7  
8  
9  
10  
11  
12  
13  
14  
15  
16  
17  
18  
19  
20  
21  
22  
23  
24  
25  
26  
27  
28  
29  
30  
31  
32  
33  
34  
35  
36  
37  
38  
39  
40  
41  
42  
43  
44  
45  
46  
47  
48  
49  
50  
51  
52  
53  
54  
55  
56  
57  
58  
59  
60

Metal phosphides are a promising class of materials that show excellent reactivity in hydrodesulfurization, hydrodenitrogenation, and hydrodeoxygenation (HDO) [40-42]. The phosphides have physical properties similar to those of both ceramics such as high strength and hardness, and of metals such as good thermal and electrical conductivity. The catalysts provide active sites that facilitate hydrogenation, hydrogenolysis as well as nucleophilic substitution. Moreover, the relatively strong metal to phosphorus interaction enhances the phosphides' resistance to S- or N- compounds. It has been shown that Ru<sub>2</sub>P/SiO<sub>2</sub> is nearly three times more active than Ru/SiO<sub>2</sub> and significantly more active than the traditional hydrotreating catalyst CoMo/Al<sub>2</sub>O<sub>3</sub> in the HDO of furan [39]. The phosphide catalysts show preference towards hydrogenolysis products, i.e. C<sub>4</sub> hydrocarbons while the metal catalysts favor decarbonylation products, i.e. C<sub>3</sub> hydrocarbons. The HDO of 2-methyltetrahydrofuran on phosphide catalysts shows higher reactivity than Ru/C and Pd/Al<sub>2</sub>O<sub>3</sub> [35,36,37,38]. The proposed reaction network involves the adsorption of 2-MTHF on a metallic site, followed by a rate-determining opening of the ether ring to produce the adsorbed intermediates 1-pentoxide or 2-pentoxide, depending on which side the ring is opened. Similar reactions occur with 2-methyltetrahydropyran on Ni<sub>2</sub>P/SiO<sub>2</sub> (*vide infra*) but with distinctive differences, such as lower reactivity.

## 2. Experimental

### 2.1 Synthesis of 2-methyltetrahydropyran

Amounts (~250 mL) of 2-methyltetrahydropyran (2-MTHP) were synthesized in three steps. First, hydrogen chloride was added to the starting material, 3,4-dihydro-2H-pyran (DHP)

1  
2  
3 to produce 2-chlorotetrahydropyran (Cl-THP), second, the Grignard reagent was prepared, and  
4  
5 third, the Grignard reagent was reacted with 2-chlorotetrahydropyran to produce 2-  
6  
7 methyltetrahydropyran as final product. Details are given in the Supplementary Information.  
8  
9

## 14 2.2 Materials and characterization

17  
18 The Ni<sub>2</sub>P catalyst was synthesized via temperature programmed reduction of a phosphate  
19  
20 precursor. Details of the method were reported earlier [35, 43, 44]. Briefly, 2 mL of an aqueous  
21  
22 solution containing 337 mg of nickel (II) nitrate (Ni(NO<sub>3</sub>)<sub>2</sub>·6H<sub>2</sub>O – Alfa Aesar, 99.6%) and 306  
23  
24 mg of ammonium hydrogen phosphate ((NH<sub>4</sub>)<sub>2</sub>HPO<sub>4</sub> – Aldrich) was impregnated onto 1 g of  
25  
26 silica (Cab-osil ® EH5). After drying at 120 °C for 4 h and calcining at 600 °C for 6 h, the  
27  
28 mixture was cooled and then pressed and pelletized to 16/20 mesh size (0.8-1.2 mm in diameter)  
29  
30 particles. The precursor particles were reduced to nickel phosphide in a H<sub>2</sub> stream (1 L min<sup>-1</sup> of  
31  
32 H<sub>2</sub> per gram of precursor) as the temperature was increased from 25 °C to 615 °C at a rate of 3 °C  
33  
34 min<sup>-1</sup>. After reduction the sample was cooled to room temperature in a He stream and was  
35  
36 passivated in a 0.5 % O<sub>2</sub>/He stream for 2 h.  
37  
38  
39  
40  
41

42 The surface area of the catalyst was estimated by N<sub>2</sub> physisorption using the Brunauer  
43  
44 Emmett Teller (BET) method. The active phase of nickel phosphide was determined by X-ray  
45  
46 diffraction and the surface sites were quantified by carbon monoxide (CO) chemisorption.  
47  
48  
49

50 The amount of acid sites on the catalyst was probed by temperature programmed  
51  
52 desorption of ammonia. First a sample of 100 mg of passivated Ni<sub>2</sub>P/SiO<sub>2</sub> was activated in H<sub>2</sub>  
53  
54 (100 cm<sup>3</sup> min<sup>-1</sup>) at 500 °C (3 °C min<sup>-1</sup> heating rate) for 2 h. After the sample was cooled in He (50  
55  
56 cm<sup>3</sup> min<sup>-1</sup>) to 120 °C and held at this temperature for 0.5 h, a 10% NH<sub>3</sub>/He stream (50 cm<sup>3</sup> min<sup>-1</sup>)  
57  
58  
59  
60

1  
2  
3 was introduced for 0.5 h. The saturated sample was flushed with pure He ( $50 \text{ cm}^3 \text{ min}^{-1}$ ) for 0.5 h  
4  
5 and then the temperature was increased from  $120 \text{ }^\circ\text{C}$  to  $700 \text{ }^\circ\text{C}$  at a heating rate of  $10 \text{ }^\circ\text{C min}^{-1}$ .  
6  
7

8 Masses 16 and 17 were monitored during the desorption by a mass spectrometer.  
9  
10

### 11 12 13 14 **2.3 Reactivity studies** 15

16  
17 For the reactivity tests of 2-methyltetrahydropyran (2-MTHP), an amount of  $\text{Ni}_2\text{P/SiO}_2$   
18 equivalent to  $12.6 \text{ } \mu\text{mol}$  of active sites was mixed with 1.5 g of quartz chips of the same size and  
19 the mixture was packed in a tubular quartz reactor of 8 mm in diameter. The catalyst was re-  
20 activated in  $\text{H}_2$  with the temperature raised from  $25 \text{ }^\circ\text{C}$  to  $500 \text{ }^\circ\text{C}$  ( $5 \text{ }^\circ\text{C min}^{-1}$ ) and held at this  
21 level for 2 h, followed by cooling to  $350 \text{ }^\circ\text{C}$ . A liquid pump was used to inject a solution of 96  
22 mol% 2-MTHP and 4 mol% benzene as internal standard at a rate of  $0.02 \text{ g min}^{-1}$  ( $3.5 \text{ } \mu\text{mol s}^{-1}$   
23 total) into a vaporizer kept at  $300 \text{ }^\circ\text{C}$  where mixing with a hydrogen stream occurred. Benzene  
24 was easily distinguished in the gas chromatograms and it was verified that benzene was not  
25 hydrogenated at the reaction conditions. The feed concentration was held at 2.6 mol% of  
26 reactant in a  $\text{H}_2$  flow ( $180 \text{ cm}^3 \text{ min}^{-1}$ ,  $123 \text{ } \mu\text{mol s}^{-1}$ ). The catalyst was stabilized for 12 h after the  
27 introduction of 2-MTHP then temperature was varied in the following order:  $350 \text{ }^\circ\text{C} \rightarrow 400 \text{ }^\circ\text{C}$   
28  $\rightarrow 450 \text{ }^\circ\text{C} \rightarrow 500 \text{ }^\circ\text{C} \rightarrow 475 \text{ }^\circ\text{C} \rightarrow 425 \text{ }^\circ\text{C} \rightarrow 375 \text{ }^\circ\text{C} \rightarrow 350 \text{ }^\circ\text{C}$ , with the temperature held for 3h  
29 at each temperature. The components in the exit stream were analyzed with a gas chromatograph  
30 equipped with a flame ionization detector and an HP-1 (0.25mm x 100m) column. In the  
31 experiments, the contact time was kept constant at 3.9 s. Contact time is defined as  $\tau = \frac{L}{F_{A0}}$ , in  
32 which  $\tau$  is the contact time (s) based on active sites,  $F_{A0}$  is the molar flow rate of 2-MTHP ( $3.2$   
33  $\mu\text{mol s}^{-1}$ ),  $L$  is the number of active sites ( $12.6 \text{ } \mu\text{mol}$ ) approximated by the CO uptake ( $45 \text{ } \mu\text{mol}$   
34  
35  
36  
37  
38  
39  
40  
41  
42  
43  
44  
45  
46  
47  
48  
49  
50  
51  
52  
53  
54  
55  
56  
57  
58  
59  
60

1  
2  
3  
4  $\text{g}^{-1} \times 0.28 \text{ g}$ ). Note that the contact time based on catalyst bed volume  $\tau_V = \frac{V}{v}$  has a value of 0.5 s,  
5  
6 where V is the bed volume ( $1.5 \text{ cm}^3$ ) and v is the volumetric flow rate ( $180 \text{ cm}^3 \text{ min}^{-1}$ ).  
7  
8

9  
10 The contact time study for 2-MTHP reactions was carried out in the same manner, except  
11 at a fixed temperature of  $450 \text{ }^\circ\text{C}$  and various contact times from 0.6 to 14.0 s. The contact time  
12 was adjusted by changing the flow rate of the feed while keeping the feed concentration constant.  
13  
14  
15  
16

17  
18 For the reactivity tests of 2-methyltetrahydrofuran (2-MTHF) a catalyst amount  
19 equivalent to  $30 \text{ } \mu\text{mol}$  of active sites mixed with 1.5 g of quartz chips were packed into a quartz  
20 tubular reactor. The catalyst was pretreated in the same manner as with 2-MTHP. A stream of  
21 3.3 mol% 2-MTHF in  $\text{H}_2$  ( $200 \text{ cm}^3 \text{ min}^{-1}$ ) made by flowing  $\text{H}_2$  through a bubbler carried 2-  
22 MTHF to the reactor. The bubbler had 95 volume% of 2-MTHF and 5 volume% of heptane as  
23 internal standard and was kept at  $0 \text{ }^\circ\text{C}$ . The n-heptane was easily distinguished in the gas  
24 chromatograms and it was verified that it did not undergo cracking at the reaction conditions.  
25  
26 The reaction was stabilized for 12h then temperature was varied as follows:  $350 \text{ }^\circ\text{C} \rightarrow 300 \text{ }^\circ\text{C} \rightarrow$   
27  $250 \text{ }^\circ\text{C} \rightarrow 275 \text{ }^\circ\text{C} \rightarrow 325 \text{ }^\circ\text{C} \rightarrow 350 \text{ }^\circ\text{C} \rightarrow 375 \text{ }^\circ\text{C}$ , with each temperature was held for 4 h. The  
28 contact time was kept at 6.8 s. The contact time of the 2-MTHP was lower at 3.9 s. It would  
29 have been better to have used the same contact time, but it's lower reactivity was unexpected,  
30 and there were supply limitations because of the need for a lengthy synthesis. In fact, we do not  
31 recommend studies of 2-MTHP because of this preparation limitation (it is not available  
32 commercially) and the complexity of the product mixture.  
33  
34  
35  
36  
37  
38  
39  
40  
41  
42  
43  
44  
45  
46  
47  
48  
49  
50

51 Mathematical modelling was carried out to evaluate the proposed reaction network.  
52 Assuming that the reactions were first-order, a set of ordinary differential equations (ODEs)  
53 describing the consumption rate of 2-MTHP (A) and the formation rates of products ( $\text{P}_i$ ) was  
54  
55  
56  
57  
58  
59  
60

1  
2  
3  
4 established, following a general form of  $\frac{d[A]}{dt}$  or  $\frac{d[P_i]}{dt} = f(k_i, [A], [P_i])$  where  $k_i$  are the  
5  
6 corresponding rate constants and  $[A]$  and  $[P_i]$  are the gaseous concentration of the reactant 2-  
7  
8 MTHP and the products in the effluent stream. The surface reactions involving adsorbed reactant  
9  
10  $A^*$  and surface species  $P_i^*$  were also modelled in a similar manner,  $\frac{d[A^*]}{dt}$  or  $\frac{d[P_i^*]}{dt} =$   
11  
12  $g(k_i, [A], [P_i], [*], [A^*], [P_i^*])$  where  $[A^*]$  and  $[P_i^*]$  are the surface concentration of the  
13  
14 adsorbates. The concentration of total active sites was set constant and equal to the sum of vacant  
15  
16 sites  $[*]$  and occupied sites  $[A^*]$  and  $[P_i^*]$ . Details of the modelling equations, initial conditions,  
17  
18 and units are given in the supplementary information. A programming language, Python 2.7, was  
19  
20 used to solve the ODEs simultaneously while adjusting the rate constants to minimize the  
21  
22 difference between the experimental data and the simulated data. The objective function for the  
23  
24 minimization was the sum of time-weighted residuals:  $SS_{tres} = \sum_i t_i^{-0.5} (f_i - y_i)^2$  where  $t_i$  is the  
25  
26 contact time value,  $f_i$  is the predicted data, and  $y_i$  is the experimental data. The function was  
27  
28 defined so as to achieve better fitting at lower contact times. Two minimization methods were  
29  
30 applied: 1. the sequential least square programming method, SLSQP, and 2. the limited-memory  
31  
32 Broyden-Fletcher-Goldfarb-Shanno, L-BFGS-B, method.

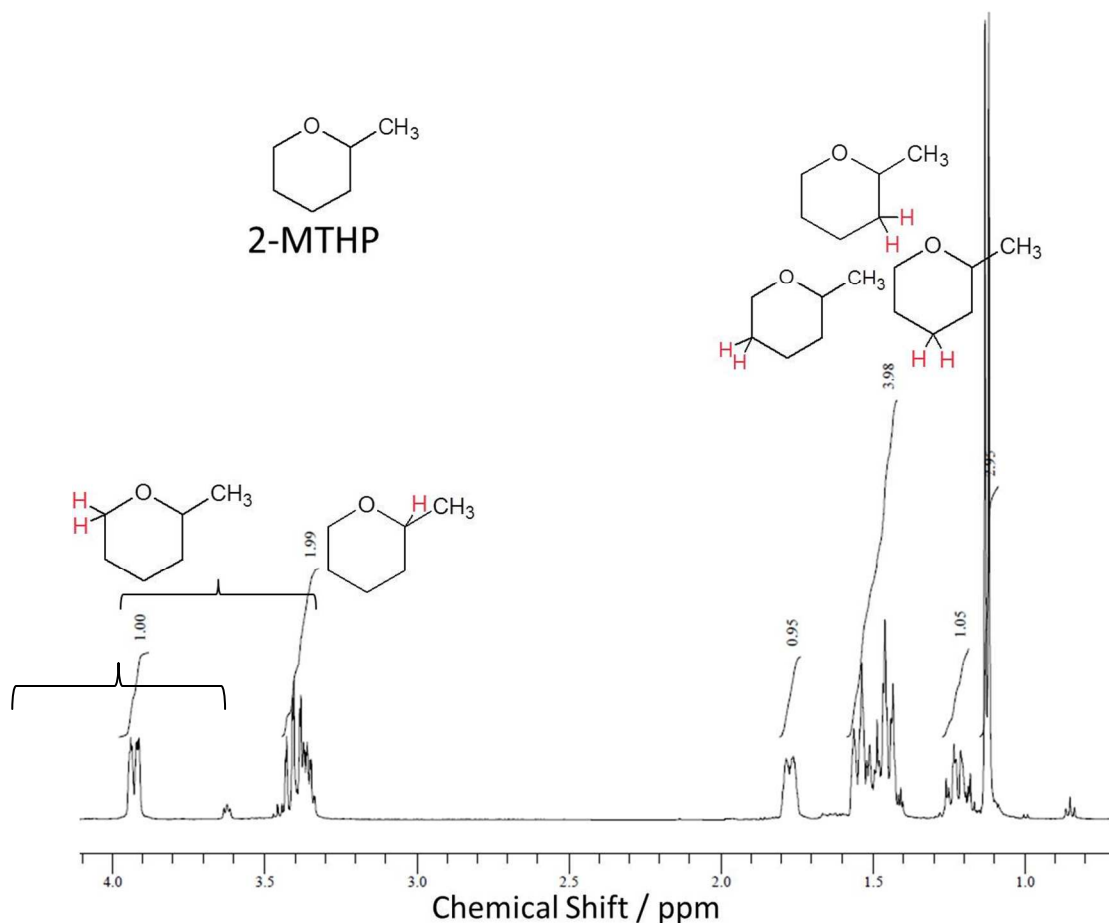
33  
34  
35  
36  
37  
38  
39  
40 The fit between the model and experimental data was reported using the coefficient of  
41  
42 determination defined as  $R^2 = \frac{SS_{reg}}{SS_{res} + SS_{reg}}$  where  $SS_{reg}$  is the regression sum of squares and  $SS_{res}$   
43  
44 is the residual sum of squares. The regression sum of squares expresses the variance of the  
45  
46 model's predictions to the observed data:  $SS_{reg} = \sum_i (f_i - \bar{y})^2$  where  $f_i$  is the predicted value and  
47  
48  $\bar{y}$  is the mean of the observed data. The residual sum of squares shows the difference between  
49  
50 the predicted data and the experimental data:  $SS_{res} = \sum_i (f_i - y_i)^2$  in which  $f_i$  is the predicted  
51  
52  
53  
54  
55  
56  
57  
58  
59  
60

1  
2  
3 value and  $y_i$  is the experimental data. The  $R^2$  value has a range from 0 to 1. A good fit occurs  
4  
5 when the  $SS_{\text{res}}$  value is minimized and so the  $R^2$  value is maximized ( $\sim 1$ ).  
6  
7  
8  
9  
10  
11  
12  
13  
14

### 15 **3 Results and Discussion**

#### 16 **3.1 Synthesis of 2-methyltetrahydropyran**

17  
18  
19  
20 For the synthesis of 2-methyltetrahydropyran the first step consisted of the addition of  
21  
22 hydrogen chloride (HCl) to the starting material 3,4-dihydro-2H-pyran (DHP) under dry  
23  
24 conditions to avoid water addition to the double bond. A yield of 90% of the 2-Cl-THP product  
25  
26 was obtained, the  $^1\text{H}$  NMR spectrum of which is shown in the Supplementary Information. The  
27  
28 2-Cl-THP product was converted to the 2-MTHP by use of a methyl Grignard reagent.  
29  
30  
31  
32  
33  
34  
35  
36  
37  
38  
39  
40  
41  
42  
43  
44  
45  
46  
47  
48  
49  
50  
51  
52  
53  
54  
55  
56  
57  
58  
59  
60



36 **Figure 1.**  $^1\text{H}$  NMR spectra of 2-methyltetrahydropyran.

37  
38  
39  
40 The proton NMR spectrum of the 2-MTHP (Figure 1) shows strong proton peaks of the  
41 methyl group at 1.1 ppm, followed by protons of the methylene groups of aliphatic carbons at  
42 1.8~1.2 ppm, and finally the protons of the alpha carbons at 3.4 and 3.9 ppm. The spectrum  
43  
44  
45  
46  
47 confirms the successful synthesis of 2-MTHP.  
48  
49  
50

### 51 52 53 54 **3.2 Characterization and reactivity results**

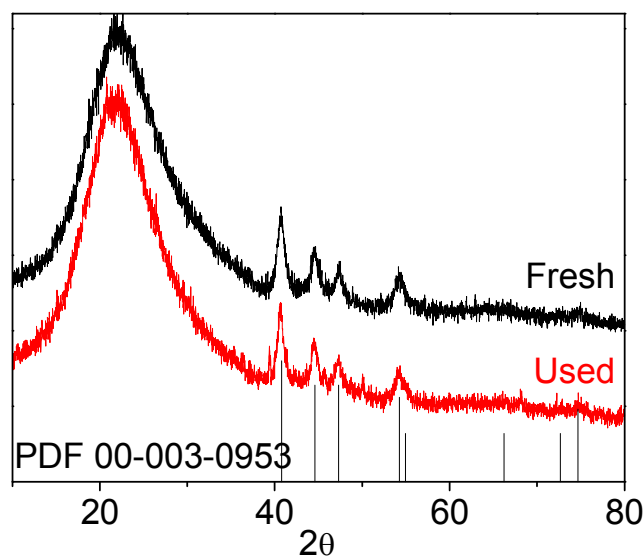


**Figure 2. X-ray diffraction pattern of Ni<sub>2</sub>P/SiO<sub>2</sub> before (top) and after (bottom) reactions.**

The synthesized Ni<sub>2</sub>P/SiO<sub>2</sub> had a BET surface area of 138 m<sup>2</sup> g<sup>-1</sup>, a CO uptake of 45 μmol g<sup>-1</sup> and a NH<sub>3</sub> uptake of 202 μmol g<sup>-1</sup>. The phosphide phase showed signature XRD peaks at 42, 44, 47, and 55 °, confirming its presence on the catalyst (Figure 2). After reaction, the crystal structure of Ni<sub>2</sub>P/SiO<sub>2</sub> was retained, indicating stability throughout the reactions (Figure 2). From the Scherrer equation the crystallite size of the reduced, passivated catalyst was 10 nm and that of the used catalyst was 11 nm. In accordance with this, the surface area decreased from 138 to 121 m<sup>2</sup> g<sup>-1</sup> and the CO uptake from 45 to 27 μmol g<sup>-1</sup>, indicating some sintering and blockage of the support and some loss of active sites during the reactions. Previous studies on guaiacol deoxygenation showed the nickel phosphide catalyst was slightly oxidized to nickel phosphate over the silica support, one of the reasons leading to the loss of active sites [7].

1  
2  
3 At atmospheric pressure, the conversion of 2-MTHP increased with increasing  
4 temperature as expected (Figure 3). The six-membered cyclic oxygenate showed a low reactivity  
5 even though the reaction temperatures were in a moderate to high range. For example, the total  
6 conversion was less than 10 % at temperatures up to 400 °C and rose to the highest 41 % at the  
7 maximum tested temperature of 500 °C. Using the same catalyst system, 2-MTHF, a five-  
8 membered ring compound homologous with 2-MTHP, showed a much higher reactivity with a  
9 total conversion over 90 % at 325 °C.  
10  
11  
12  
13  
14  
15  
16  
17  
18  
19

20  
21 Turnover frequency indicates the amount of reactant converted per surface metal atom  
22 active site as estimated by CO chemisorption and gives a useful estimate of the intrinsic  
23 reactivity of the catalyst. The turnover frequency is calculated as  $TOF = \frac{F_{A0}X}{L 100}$ , where  $F_{A0}$  is the  
24 molar flow rate of 2-MTHP ( $3.2 \mu\text{mol s}^{-1}$ ), X is total conversion (%), and L is the number of  
25 active sites ( $12.6 \mu\text{mol}$ ). The profiles of turnover frequency of 2-MTHP and 2-MTHF are shown  
26 in the bottom graph of Figure 3. The observed trend reflects the conversion profile, which  
27 showed a lower reactivity of 2-MTHP compared to 2-MTHF. It should be noted that the contact  
28 time for 2-MTHP (3.9 s) was shorter than for 2-MTHF (6.8 s), so 2-MTHP molecules had less  
29 time to approach and interact with the active sites. This difference in contact time could give at  
30 most a factor of two greater conversion of 2-MTHF and does not account for the reactivity  
31 difference (*vide infra*).  
32  
33  
34  
35  
36  
37  
38  
39  
40  
41  
42  
43  
44  
45  
46  
47

48 The Arrhenius plots are linear at low temperature, and the apparent activation energies  
49 were  $133 \text{ kJ mol}^{-1}$  for 2-MTHP and  $116 \text{ kJ mol}^{-1}$  for 2-MTHF. The slightly higher value for 2-  
50 MTHP can be attributed to the lower ring strain, and thus lower ground state energy, of 2-MTHP  
51 that possesses a six-membered ring compared to 2-MTHF [45]. This results in a relatively larger  
52 activation energy in the ring opening reaction of 2-MTHP compared to 2-MTHF. At high  
53  
54  
55  
56  
57  
58  
59  
60

1  
2  
3 temperature the turnover frequencies of both molecules level off due to mass transfer limitations  
4  
5 (Figure 3). To compare the reactivity at the same temperature, for example at 400 °C, the  
6  
7 turnover frequency of 2-MTHF can be extrapolated and it is found to be about two orders of  
8  
9 magnitude larger than that of 2-MTHP at this temperature. The difference can be attributed to the  
10  
11 ring size and the ring-strain energy of the compounds. For instance, tetrahydropyran with a six-  
12  
13 membered ring is reported to have a strain energy of 2.1 kJ mol<sup>-1</sup> while tetrahydrofuran with a  
14  
15 five-membered ring has a strain energy of 24.7 kJ mol<sup>-1</sup> [45]. Thus, for 2-MTHP ring opening is  
16  
17 not as favorable as for 2-MTHF, and higher temperatures are needed. The 2-MTHF is a less-  
18  
19 hindered *O*-ligand, because the molecule's planar structure has the neighboring H-atoms pointing  
20  
21 away from the oxygen atom, while the 2-MTHP in the chair conformation has two of the H-  
22  
23 atoms pointing in the same direction as the oxygen atom. The geometry causes tetrahydrofuran  
24  
25 to have a smaller dipole moment of 1.74 compared to tetrahydropyran which has a dipole  
26  
27 moment of 1.87 [46]. The nonplanarity of the 2-MTHP may lead to weaker binding and easier  
28  
29 desorption from catalytic sites.  
30  
31  
32  
33  
34  
35  
36  
37  
38  
39  
40  
41  
42  
43  
44  
45  
46  
47  
48  
49  
50  
51  
52  
53  
54  
55  
56  
57  
58  
59  
60

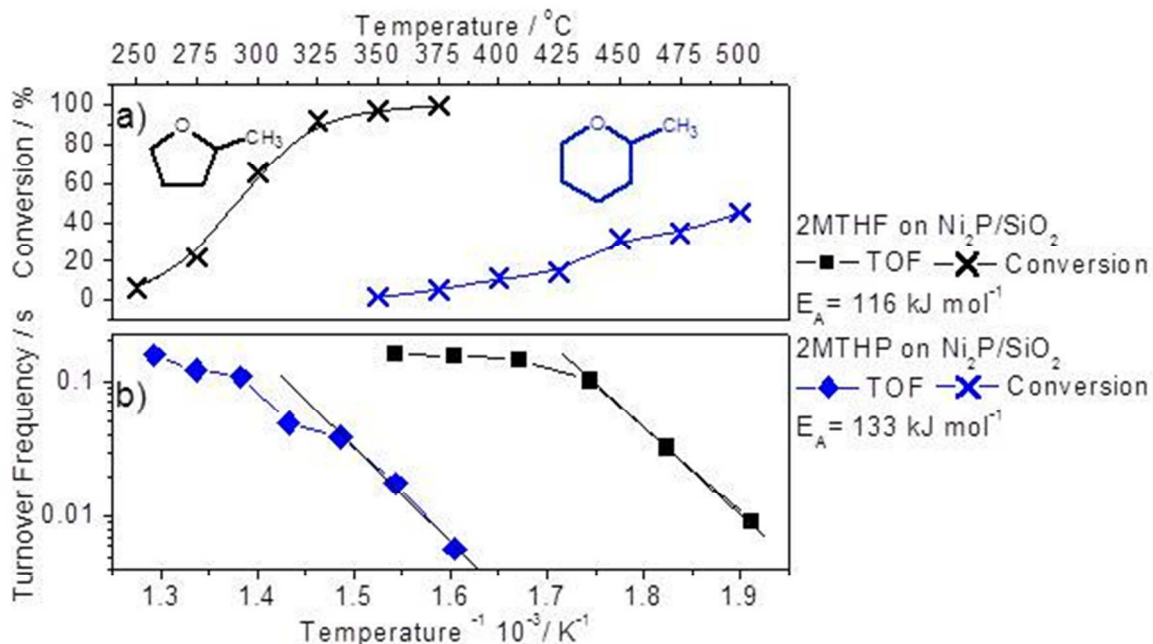


**Figure 3. Reactivity of 2-MTHP and 2-MTHF on Ni<sub>2</sub>P/SiO<sub>2</sub> in H<sub>2</sub>, 1 atm: a) conversion vs. temperature and b) turnover frequency vs. inverse temperature.**

A Weisz-Prater analysis was carried out for all reactivity experiments to determine the influence of pore diffusion on the reaction rates. The detailed analysis is provided in the Supplementary Information (SI). In Figure 3a, the lower conversion data satisfied the Weisz-Prater criterion ( $C_{WP}$ ), indicating that internal diffusion limitations were negligible, whereas, the higher conversion data for 2-MTHF showed values of  $C_{WP}$  of  $\sim 1.4$ , indicating mass transfer limitations [47,48]. The Arrhenius plots in Figure 3b duly showed a flatter region for the higher temperature, higher conversion points on the left side of each plot, characteristic of diffusion limitations. It should be noted that the contact time studies to be presented later were carried out in the kinetic regime.

1  
2  
3 The reactions of 2-MTHP on Ni<sub>2</sub>P/SiO<sub>2</sub> produced mostly unsaturated products (Figure 4).  
4  
5 This result is understandable thermodynamically since dehydrogenation is generally favored at  
6  
7 high temperatures and the reactions of 2-MTHP at 1 atm occurred only at high temperatures  
8  
9 (Figure 3). The products included C1-C4 hydrocarbons (6 %), 2-pentenes (10 %), 2-hexene  
10  
11 (49 %), 2-hexanone (19 %), and dehydrogenated pyran derivatives (11%). Some hex-4-enal and  
12  
13 hex-4-en-1-ol (3%) were formed at temperatures lower than 450 °C but were not observed at  
14  
15 higher temperatures. Analogous products were observed from the reactions of 2-MTHF such as  
16  
17 the cracking product, *n*-butane, the deoxygenation product, *n*-pentane, and the ketone, 2-  
18  
19 pentanone. All of these products had saturated hydrocarbon chains, and in fact, very few  
20  
21 unsaturated products were produced with the reactant 2-MTHF in contrast to 2-MTHP. This is  
22  
23 partly because reactions of 2-MTHF proceeded at much lower temperatures with conversion  
24  
25 more than 60% at 300 °C, where hydrogenation reactions dominated.  
26  
27  
28  
29  
30  
31

32 As temperature was raised, 2-MTHP was converted to increasing amounts of C5 products  
33  
34 like 2-pentenes and decreasing quantities of deoxygenated products like 2-hexenes, suggesting  
35  
36 that decarbonylation was favored with increasing temperatures. At the same time, the alcohol  
37  
38 species, mostly primary, diminished while 2-hexanone remained significant. This indicates that  
39  
40 these two species were formed by independent pathways.  
41  
42  
43  
44

45 The product distribution for the reaction of 2-MTHP indicates that ring opening can  
46  
47 occur on both sides of the oxygen atom to give rise to primary-substituted (e.g. 1-hexenal/ol) and  
48  
49 secondary-substituted (e.g. 2-hexanone) products. These different pathways will be denoted as  
50  
51 Path I for the primary products and Path II for the secondary products in subsequent discussion.  
52  
53  
54 Overall at conditions similar to those of fast pyrolysis with low contact time and high  
55  
56 temperatures, the total deoxygenation of 2-MTHP attained moderately high levels of 70%.  
57  
58  
59  
60

Higher deoxygenation levels require higher pressures, but not too high as 0.5 MPa already gives >98% deoxygenated products for 2-MTHF at 300 °C [37].

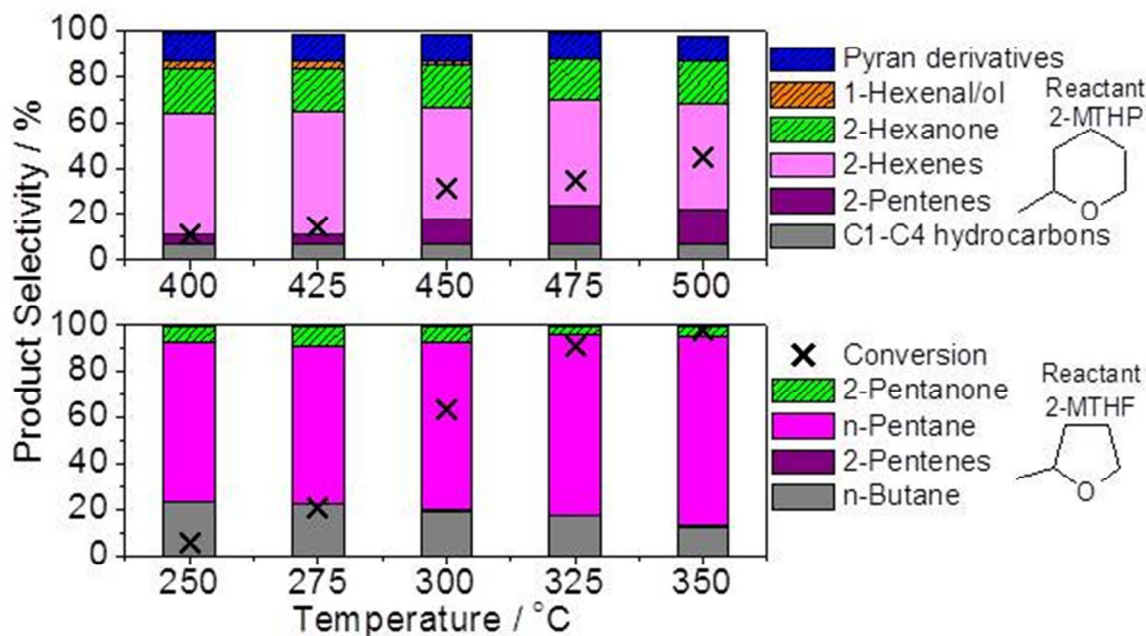


**Figure 4. Product selectivities of reactions of 2-MTHP (top) and 2-MTHF (bottom) on Ni<sub>2</sub>P/SiO<sub>2</sub> at 0.1 MPa.**

### 3.3 Simple reaction network

The reaction sequence of 2-MTHP on Ni<sub>2</sub>P/SiO<sub>2</sub> can be inferred from the results of contact time measurements where the product selectivities reveal the sequence of product formation. Initial products are formed first and thus show non-zero selectivities at short contact time that decrease with increasing contact time. Intermediate products are produced from the initial species so they start out at zero then increase to a maximum before finally abating as they form final products. Final products in the sequence also start at zero but rise steadily with

1  
2  
3 contact time. In **Figure 5** the selectivities (left) and yields (right) of the products are presented  
4  
5 for the four main groups: a) initial oxygenated products produced from the ring-opening on the  
6  
7 methyl substituted side, in Path I: hex-4-en-1-ol and hex-4-enal, b) intermediate oxygenated  
8  
9 products from the ring-opening on the unsubstituted side, in Path II: 2-hexanone, c) final  
10  
11 deoxygenated products: 2-hexenes and 2-pentenes, and d) dehydrogenated products. The total  
12  
13 conversion (indicated by the symbol X) is also shown in panel d). The curves presented are  
14  
15 results from a simple kinetic analysis to be discussed later.  
16  
17  
18  
19

20  
21 On the left side of **Figure 5**, the primary alcohol, hex-4-en-1-ol, and the aldehyde, hex-4-  
22  
23 enal, showed decreasing selectivities and yields with increasing contact time, exhibiting apparent  
24  
25 initial product behavior. However, the amounts formed are very small (see scale on left of  
26  
27 figure), and it's difficult to make an exact determination. In contrast, the ketone, 2-hexanone,  
28  
29 exhibited increasing selectivity with contact time, and with high selectivities and yields. The  
30  
31 deoxygenated products, 2-hexenes and 2-pentenes, also demonstrated the same trends. On the  
32  
33 right side of **Figure 5**, the yields of 2-hexanone, 2-hexenes, and 2-pentenes rose slowly at first  
34  
35 when contact time was less than 4 s, then increased rapidly. This growth lag at the start suggests  
36  
37 that these products were formed later in the sequence. The secondary alcohol 2-hexanol was not  
38  
39 detected in the gas phase probably because its formation amount was below the detection limit,  
40  
41 as a result of the compound's affinity for the active sites that inhibited desorption. Meanwhile,  
42  
43 the formation of 2-hexanone was preferred, with the desorption of 2-hexanone being dominant.  
44  
45  
46  
47 The pyran derivatives included mostly dehydrogenated products and a small amount of  
48  
49 isomerized products of 2-MTHP, which probably existed in equilibrium with 2-MTHP.  
50  
51  
52  
53  
54  
55  
56  
57  
58  
59  
60

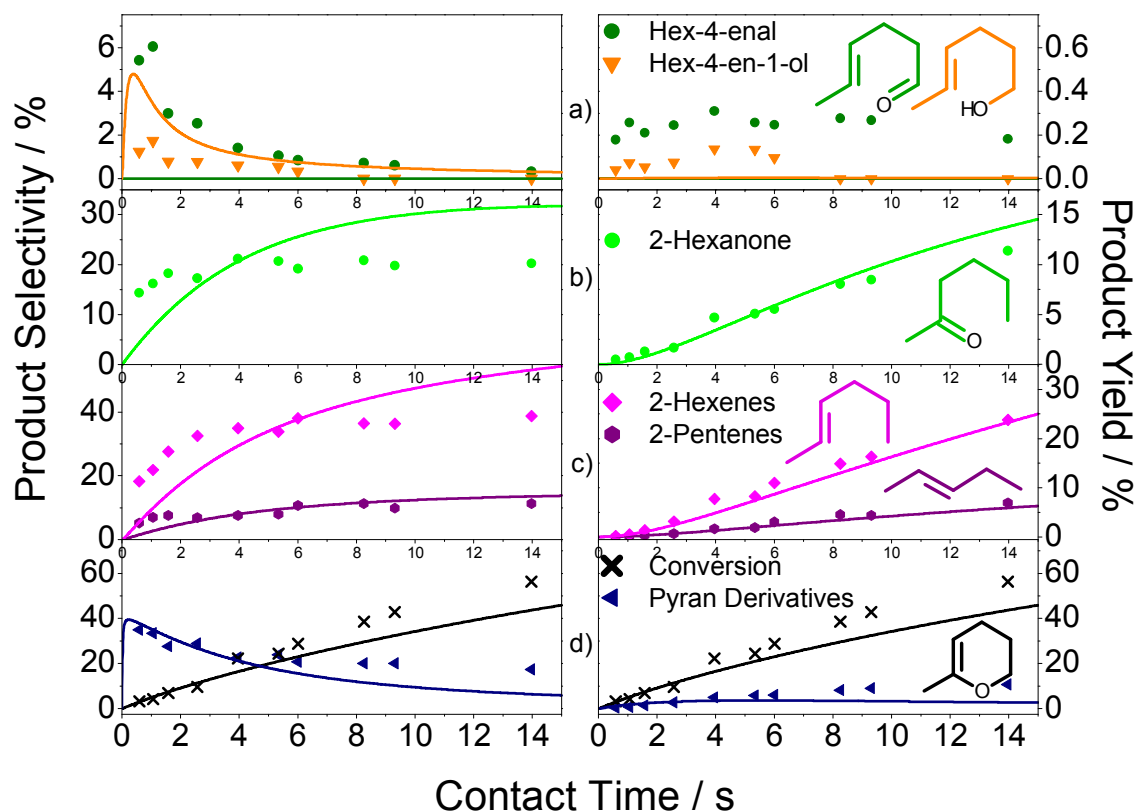
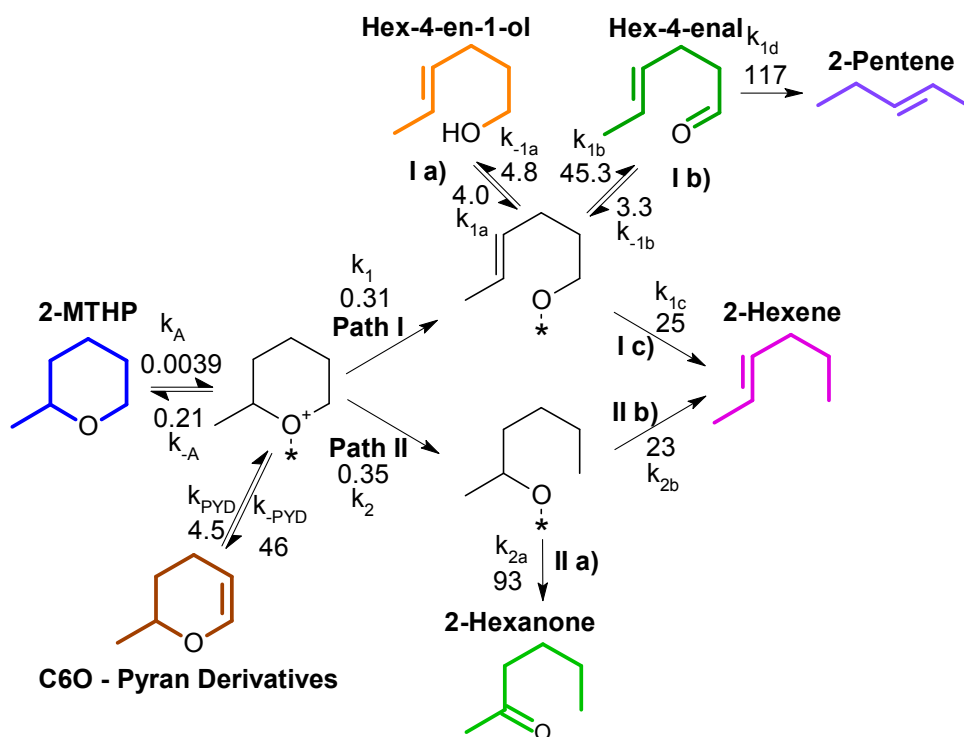


**Figure 5. Contact time study of 2-MTHP reactions on  $\text{Ni}_2\text{P}/\text{SiO}_2$  in  $\text{H}_2$  at 0.1 MPa, 450 °C. Points are experimental data and lines are calculated using the rate constants in Scheme 1. a) Product selectivity and yield for hex-4-enal and hex-4-en-1-ol, b) Product selectivity and yield for 2-hexanone, c) Product selectivity and yield for 2-hexenes and 2-pentenes, d) Product selectivity and yield for pyran derivatives and conversion of 2-MTHP**

Based on the contact time results, a preliminary reaction sequence is proposed as follows (Scheme 1). The first step is the adsorption of 2-MTHP on an active site followed by ring-opening to give either primary or secondary alkoxide species depending on the cleavage position of the intra-ring C-O bond. The adsorbed primary alkoxide species in Path I, formed from ring-opening on the methyl-substituted side, undergoes the following reactions: I a) protonation to

yield a primary alcohol, I b) hydrogen elimination to give an aldehyde which can be decarbonylated in a later step to 2-pentene, and I c) deoxygenation to 2-hexene. In path II, the adsorbed secondary alkoxide produced from cleavage on the unhindered side can II a) eliminate hydrogen to give 2-hexanone or can be II b) dehydrated to 2-hexene.



**Scheme 1.** Proposed simple reaction network of 2-MTHP on  $\text{Ni}_2\text{P}/\text{SiO}_2$ , 1atm, 450 °C. Gas phase species are shown in color, adsorbed species are in black. The rate constant values are indicated. Units are  $\text{s}^{-1}$  for the surface reaction and desorption rate constants and  $\text{cm}^3 \mu\text{mol}^{-1} \text{s}^{-1}$  for the adsorption rate constants.

Fitting results for the simple reaction network are shown in **Figure 5** and the rate constants in Table 1. The network takes into consideration the main observed gas phase species with the most minimal possible consideration of surface species. The  $R^2$  value for the fitting of

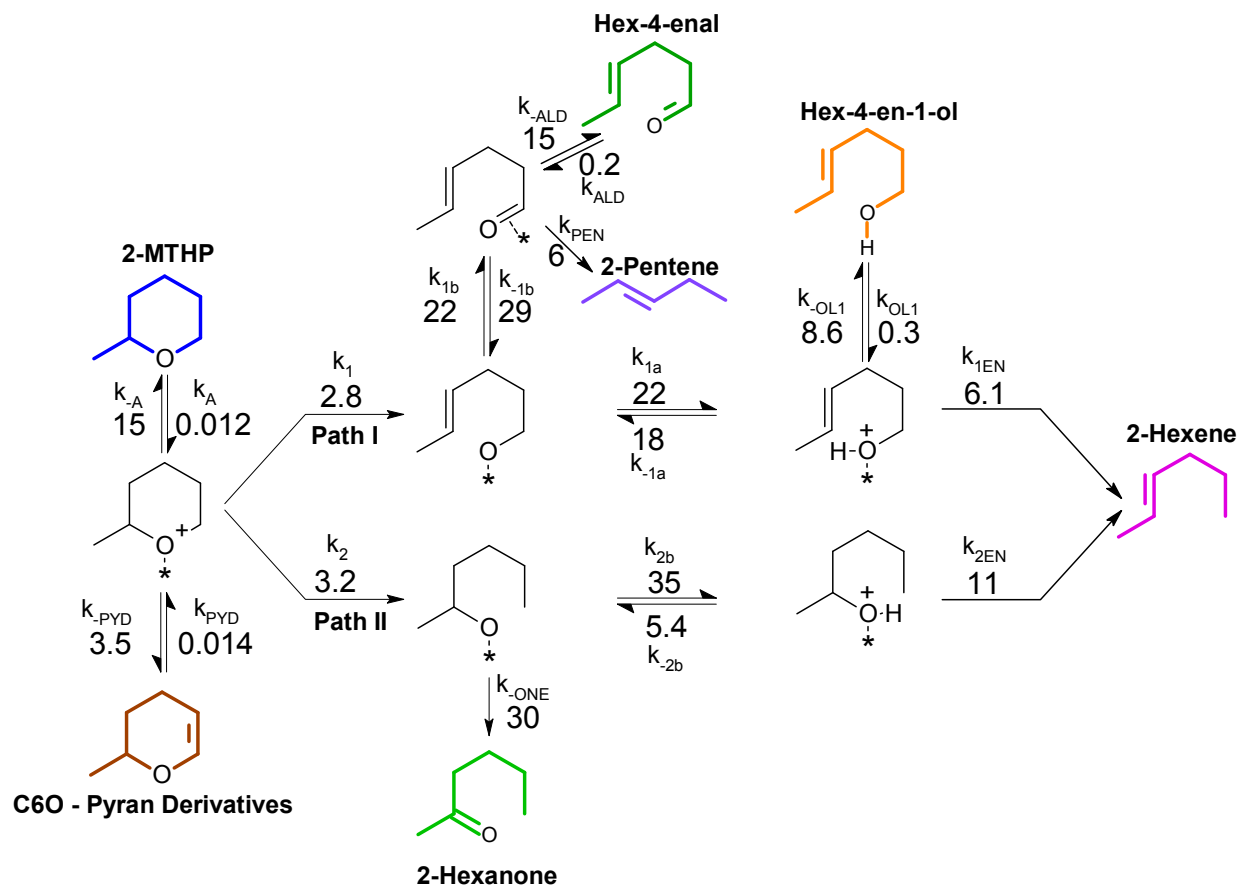
the yields was 0.78 and for the selectivities was 0.75. The results are consistent with the observation that the simulated yields of the main products, 2-hexanone, 2-hexenes and 2-pentenes match more closely to the experimental data (**Figure 5**, two middle plots on the right side) compared to the other calculated yields and selectivities. It is realized that this simple scheme is inadequate in describing the reaction of 2-MTHP on Ni<sub>2</sub>P/SiO<sub>2</sub> and that a more detailed model is required.

**Table 1: Rate constants for the simple reaction network (Scheme 1)**

Reactant		Path I							Path II				
$k_A$	$k_{-A}$	$k_1$	$k_{1a}$	$k_{-1a}$	$k_{1b}$	$k_{-1b}$	$k_{1c}$	$k_{1d}$	$k_2$	$k_{2a}$	$k_{2b}$	$k_{PYD}$	$k_{-PYD}$
0.0039	0.21	0.31	4.8	4.0	3.3	45	25	117	0.35	93	23	4.5	46
$\text{cm}^3$	$\text{s}^{-1}$	$\text{cm}^3$	$\text{s}^{-1}$										
$\mu\text{mol}^{-1}$												$\mu\text{mol}^{-1}$	
$\text{s}^{-1}$												$\text{s}^{-1}$	

### 3.4 Detailed reaction network

A comprehensive sequence is proposed in Scheme 2. The adsorbed alkoxide species progresses to form other intermediate surface species prior to desorption into the observed products. In Path I the primary alkoxide species transforms in two ways. It can convert to an adsorbed aldehyde or to an adsorbed primary alcohol. The aldehyde can desorb or go through decarbonylation into 2-pentenes and the alcohol may desorb or form 2-hexenes. In path II the secondary alkoxide species reacts to produce 2-hexanone or undergoes protonation then dehydration to generate 2-hexenes.



Scheme 2. Proposed detailed reaction network for 2-MTHP reactions on  $\text{Ni}_2\text{P}/\text{SiO}_2$  at 1atm, 450 °C. Gas phase species are shown in color, adsorbed species are in black. Units for the rate constants are  $\text{s}^{-1}$  for the surface reaction and desorption rate constants and  $\text{cm}^3 \mu\text{mol}^{-1} \text{s}^{-1}$  for the adsorption rate constants.

The fitting results for the detail scheme (Scheme 2) are plotted in **Figure 6**. The  $R^2$  value for the fitting of the yields is 0.96 and for the selectivities is 0.90. The continuous lines showing the simulation results fit the experimental points well, indicating that the proposed network is consistent with the data.

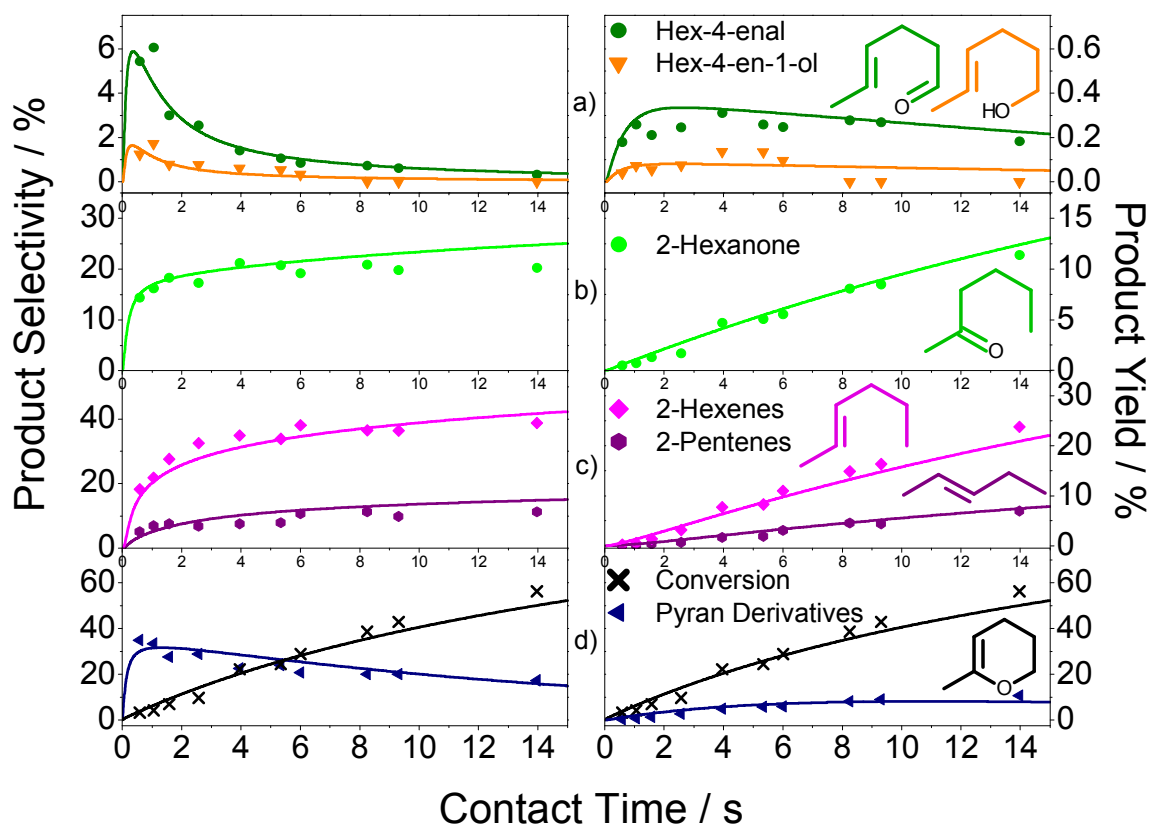


**Figure 6. Fitting results for the detailed reaction network of 2-MTHP on Ni<sub>2</sub>P/SiO<sub>2</sub> in H<sub>2</sub> at 1 atm, 450 °C. Points are experimental data and lines are simulated data using the estimated rate constants in Scheme 2. a) Product selectivity and yield for hex-4-enal and hex-4-en-1-ol, b) Product selectivity and yield for 2-hexanone, c) Product selectivity and yield for 2-hexenes and 2-pentenes, d) Product selectivity and yield for pyran derivatives and conversion of 2-MTHP.**

The estimated values for the rate constants in Scheme 2 indicate a slow adsorption of the 2-MTHP on a vacant active sites (Table 2). The ring-opening steps display the smallest values for rate constants compared to all subsequent surface reaction steps, suggesting that these are rate

determining steps. The rate constant for the ring-opening step at the less hindered side of 2-MTHP in Path II is slightly larger than the rate constant for reaction at the more hindered side of 2-MTHP in Path I. The trends of the values of rate constants observed here with the six-membered-ring 2-MTHP molecule show similarity to those of the five-membered ring of 2-MTHF. The studies of both molecules show that the ring-opening steps are rate limiting and that the ring opening is faster on the less hindered side of 2-MTHP in path II than on the hindered side.

**Table 2: Estimated rate constants for detailed reaction network (Scheme 2)**

Reactant		Surface reactions Path I						Path II				
		$k_1$	$k_{1a}$	$k_{-1a}$	$k_{1b}$	$k_{-1b}$	$k_2$	$k_{2b}$	$k_{-2b}$			
		2.8	22	18	22	29	3.2	35	5.4			
		$s^{-1}$	$s^{-1}$	$s^{-1}$	$s^{-1}$	$s^{-1}$	$s^{-1}$	$s^{-1}$	$s^{-1}$			
		Adsorption / desorption Path I						Path II				
$k_A$	$k_{-A}$	$k_{ALD}$	$k_{-ALD}$	$k_{OL1}$	$k_{-OL1}$	$k_{1EN}$	$k_{PEN}$	$k_{-ONE}$	$k_{2EN}$	$k_{PYD}$	$k_{-PYD}$	
0.012	15	0.2	15	0.3	8.6	6.1	6.0	30	11	0.014	3.5	
$cm^3$	$s^{-1}$	$cm^3$	$s^{-1}$	$cm^3$	$s^{-1}$	$s^{-1}$	$s^{-1}$	$s^{-1}$	$s^{-1}$	$cm^3$	$s^{-1}$	
$\mu mol^{-1}$		$\mu mol^{-1}$		$\mu mol^{-1}$						$\mu mol^{-1}$		
$s^{-1}$		$s^{-1}$		$s^{-1}$						$s^{-1}$		

Concentrations of the surface species are plotted in Figure 7. The results show a low adsorption of 2-MTHP on the catalyst, probably due to high temperature and low contact time. The adsorbed reactant is the dominant species, followed by the adsorbed species from Path I, and finally the adsorbed species from Path II. This order reflects the trend observed in Scheme 2 where Path I includes surface reactions and desorption steps with lower rate constants compared to those of Path II, so the intermediate species from Path I have longer residence on the active sites.

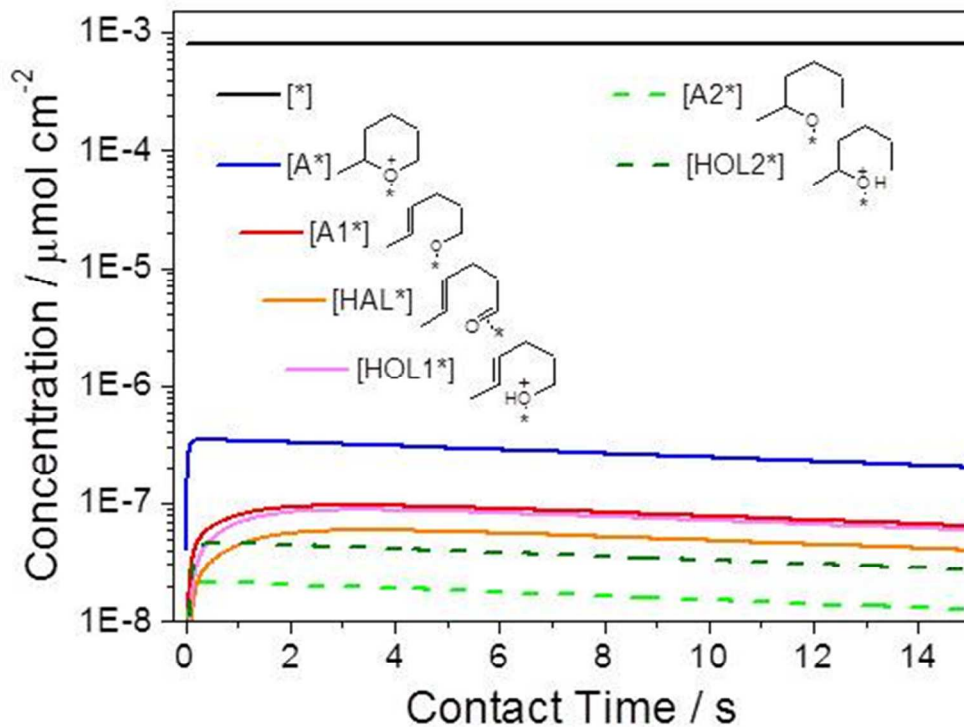


**Figure 7. Concentrations of surface species calculated from the estimated rate constants from Scheme 2.**

The nickel phosphide catalyst offers multiple active centers for hydrogen transfer and deoxygenation steps as suggested by the following discussion of the crystal structure of the catalyst [41, 49]. The metal-rich  $\text{Ni}_2\text{P}$  particles supported on silica have a crystal structure consisting of two types of Ni atoms, referred to as Ni(1) and Ni(2), as well as two types of P atoms, P(1) and P(2) [50-52]. The surface Ni atoms are positively charged by 0.07 e, and the P atoms are negatively charged by -0.07 e, so the Ni atoms provide binding sites for electron-rich adsorbates such as O-compounds. The P atoms may be associated with unreduced passivation oxygen to form acidic P-OH centers, although a recent diffuse reflectance infrared spectroscopy study suggests that at reducing conditions only the phosphate on the silica is oxidized [53]. The Ni(1) site has a near tetrahedral structure and favors hydrogenolysis reactions while the Ni(2) site

1  
2  
3 has a square pyramidal structure and prefers hydrogenation reactions [54]. The bulk structure of  
4  
5 Ni<sub>2</sub>P has alternating layers of Ni<sub>3</sub>P<sub>2</sub> and Ni<sub>3</sub>P stacked along the (0001) direction [41,55,56]. The  
6  
7 Ni<sub>3</sub>P<sub>2</sub> layer contains Ni(1) and P(2) atoms and is reported to be more stable than the Ni<sub>3</sub>P layer,  
8  
9 which has Ni(2) and P(1) atoms. The surface (0001) should be dominated with Ni<sub>3</sub>P<sub>2</sub> structure.  
10  
11 Yet, the threefold hollow sites in a Ni(1) vacancy on a Ni<sub>3</sub>P<sub>2</sub>-terminated surface lack a P  
12  
13 exposing dangling bonds that require stabilization, resulting in a surface with about 80% of P-  
14  
15 covered Ni<sub>3</sub>P<sub>2</sub> structure (or Ni<sub>3</sub>P-P structure) and 20% of uncovered Ni<sub>3</sub>P<sub>2</sub> structure [57,58]. A  
16  
17 similar conclusion was reached for the (10 $\bar{1}$ 0) plane in which all Ni atoms are P-terminated [59].  
18  
19 So, much of the active surface metallic Ni sites are covered with P atoms, leading to a much  
20  
21 lower apparent number of active sites, quantified by CO chemisorption, than the theoretical  
22  
23 value from the total surface area of Ni<sub>2</sub>P crystallites.  
24  
25  
26  
27  
28  
29

30 The Ni(1) sites are active for adsorption of *S*-compounds and *O*-compounds [41,60] and  
31  
32 are likely to be the adsorption sites for 2-MTHP and the intermediate species. Both Ni(1) and  
33  
34 Ni(2) sites could be responsible for hydrogen dissociative adsorption, assisting the ring opening  
35  
36 reactions [40,61]. Thus, both sites are involved in the reaction.  
37  
38  
39

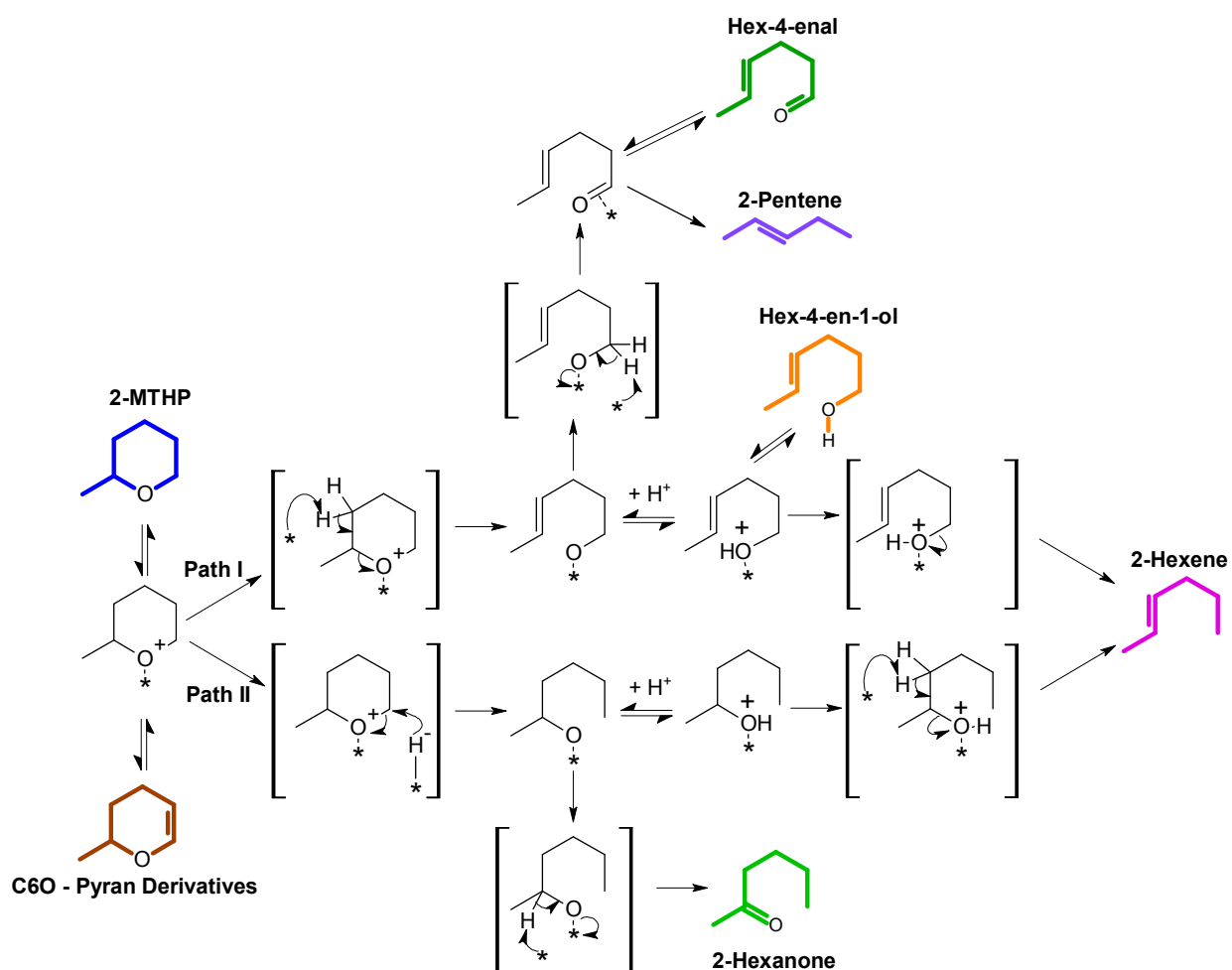
40 The role of surface P atoms is both beneficial and detrimental. The P atoms protect the  
41  
42 stability of the nickel phosphide phase and break up Ni ensemble that can produce coke; yet, an  
43  
44 excess of P atoms reduces the availability of active Ni sites. Nevertheless, theoretical studies  
45  
46 indicate that the P sites are capable of adsorbing atomic hydrogen [62, 63] which can serve as a  
47  
48 hydrogen source for various reactions. The hydrogen may spill over from nickel centers. Also,  
49  
50 in oxidized form the P atom can serve as hydrogen acceptor. Such oxidized species have been  
51  
52 observed by FT-IR spectroscopy [64]. The CO uptake was 45  $\mu\text{mol g}^{-1}$  and the NH<sub>3</sub> uptake was  
53  
54 202  $\mu\text{mol g}^{-1}$ , indicating that there are more acid sites than metal sites. The NH<sub>3</sub> adsorption  
55  
56  
57  
58  
59  
60

1  
2  
3 method does not distinguish between Brønsted and Lewis sites, so no definite conclusions can be  
4  
5 made on their role. It is speculated that the Brønsted acid sites are likely associated with oxidized  
6  
7 phosphorus both on the phosphide and any excess on the support and are involved with the  
8  
9 various proton transfer processes in the reactions of the adsorbed 2-MTHF and 2-MTHP. It is  
10  
11 also surmised that the Lewis sites are associated with reduced Ni sites which are involved in  
12  
13 interactions with the oxygen atoms in the adsorbates.  
14  
15  
16  
17

18  
19 The detailed chemistry of the subsequent steps is presented in Scheme 3. For ring  
20  
21 opening on the substituted side (Scheme 3, Path I), the reaction must involve atoms more distant  
22  
23 from the hindered side, which would have only weak interactions with the active sites due to the  
24  
25 steric blockage. So it is likely that a basic site abstracts a proton from a  $\beta$ -carbon in an E2  
26  
27 elimination, creating a hex-4-en-1-alkoxide species. This elimination requires the hydrogen to be  
28  
29 antiperiplanar with the leaving group so the 2-MTHP molecule likely reacts in a chair  
30  
31 conformation. An  $\alpha$ -hydrogen elimination from the alkoxide produces an aldehyde species. The  
32  
33 adsorbed aldehyde has a moderate interaction with the active site so it can desorb or go through a  
34  
35 decarbonylation step to produce 2-pentene. The primary alkoxide could also be protonated to  
36  
37 form an adsorbed primary alcohol. The surface adsorbed water and/or P-OH groups are possible  
38  
39 proton donors. The adsorbed alcohol could simply desorb or undergo hydrogenolysis to 2-  
40  
41 hexene. The process requires an attack by a hydride, possibly a metal hydride Ni-H<sup>-</sup>, on the  $\alpha$ -  
42  
43 carbon and a shift of the electron pair to a nearby proton, creating 2-hexene and an adsorbed  
44  
45 hydroxyl group.  
46  
47  
48  
49  
50

51  
52 The ring opening on the unsubstituted side (Scheme 3, Path II), has less steric hindrance  
53  
54 than Path I. The transformation is likely initiated by a hydride attack on the  $\alpha$ -carbon, which  
55  
56 cleaves the C-O bond in an S<sub>N</sub>2 manner, yielding an adsorbed secondary alkoxide. The 2-  
57  
58  
59  
60

hexanone is produced by abstraction of a proton by a basic site from the substituted  $\alpha$ -carbon. The secondary alkoxide can also undergo protonation and subsequent dehydration to form 2-hexene. It is interesting that no secondary alcohol was detected. This is possibly because the adsorbed secondary alcohol precursor is very reactive and readily undergoes dehydration to 2-hexene.



1  
2  
3 **Scheme 3. Proposed detailed chemistry of the surface steps in the reaction network. Gas**  
4 **phase species are shown in color, adsorbed species are in black. Symbol \* represents a**  
5 **surface site. The species in brackets depict suggested possible reaction steps.**  
6  
7  
8  
9

10  
11  
12  
13 In summary this second reaction network gives a good fit to the contact time data. It is  
14 acknowledged that the number of fitting constants is larger than the simpler scheme. However,  
15 what this indicates is that this type of analysis requires a realistic description of the elementary  
16 steps involved in a transformation. It should be recognized that confirmation of the model results  
17 is needed by independent measurements, for example, by spectroscopic observation of the  
18 adsorbed intermediates.  
19  
20  
21  
22  
23  
24  
25  
26  
27  
28  
29  
30  
31  
32

#### 33 **4. Conclusions**

34  
35

36 The six-membered ring compound 2-methyltetrahydropyran with less ring strain was  
37 much less reactive on Ni<sub>2</sub>P/SiO<sub>2</sub> than the analogous five-membered ring compound 2-  
38 methyltetrahydrofuran. At conditions similar to those of fast pyrolysis, i.e. low contact time and  
39 high temperature, nickel phosphide showed good deoxygenation capability (~70%) and produced  
40 2-hexenes and 2-pentenes at all conversion levels. The reaction routes for 2-MTHP were similar  
41 to those for 2-MTHF and involved two main pathways, depending on the C-O bond that cleaved  
42 in the first step. Cleavage on the methyl-substituted side produced linear aldehyde and primary  
43 alcohol compounds while cleavage on the unsubstituted side formed a ketone product. Both  
44 routes generated 2-hexene as final products while Path I also produced 2-pentene. Metallic Ni  
45 sites are possibly the main active sites for the adsorption of reactants and the dissociative  
46  
47  
48  
49  
50  
51  
52  
53  
54  
55  
56  
57  
58  
59  
60

1  
2  
3 adsorption of hydrogen while P-OH sites provide protons. The reaction network was supported  
4  
5 by fitting with a kinetic model. The obtained values of the rate constants showed that the slowest  
6  
7 step was ring-opening of adsorbed 2-MTHP, consistent with previous results for the homologue  
8  
9 2-MTHF.  
10  
11  
12  
13  
14  
15  
16

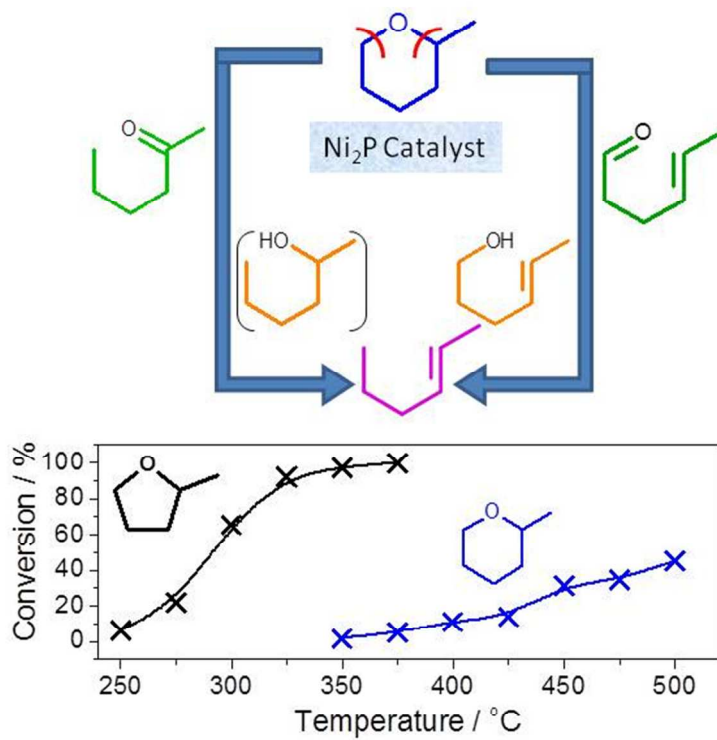
### 17 **Acknowledgments**

18  
19  
20 This work was supported by the US Department of Energy under grant DE-FG02-96ER 14669,  
21  
22 and the Japan Society for the Promotion of Science for a Grant-in-Aid for Scientific Research  
23  
24 (B) (no. 26289301).  
25  
26  
27  
28

### 29 **Supporting Materials (SI)**

30  
31 The SI section describes 1) The detailed preparation of the 2-methyltetrahydropyran compound,  
32  
33 2) Calculations of the Weisz-Prater criterion for lack of diffusion limitations, 3) The equations  
34  
35 used in the modeling of the reaction network. This material is available free of charge via the  
36  
37 Internet at <http://pubs.acs.org>.  
38  
39  
40  
41  
42  
43  
44  
45  
46  
47  
48  
49  
50  
51  
52  
53  
54  
55  
56  
57  
58  
59  
60

## Table of Contents Graphic



---

References

- 1 Maity, S. K. *Renew. Sus. Energy Rev.* **2015**, 43, 1446–1466.
- 2 Gunawardena, A. D.; Fernando, D. S. Methods and Applications of Deoxygenation for the Conversion of Biomass to Petrochemical Products. In *Biomass Now - Cultivation and Utilization* [Online]; Matovic, D. M., Ed; InTech, 2013; Chapter 11, pp 273-298. <http://www.intechopen.com/books/biomass-now-cultivation-and-utilization/methods-and-applications-of-deoxygenation-for-the-conversion-of-biomass-to-petrochemical-products> (accessed Oct 07, 2015).
- 3 Linck, M.; Felix, L.; Marker, T.; Roberts, M. *WIREs Energy Environ.* **2014**, 3, 575–581.
- 4 Pham, T. N.; Shi, D.; Resasco, D. E. *Appl. Catal., B* **2014**, 145, 10–23.
- 5 Mu, W.; Ben, H.; Ragauskas, A.; Deng, Y. *BioEnergy Res.* **2013**, 6, 1183–1204.
- 6 Arun, N.; Sharma, R. V.; Dalai, A. K. *Renew. Sus. Energy Rev.* **2015**, 48, 240–255.
- 7 Ruddy, D. A.; Schaidle, J. A.; Ferrell, J. A. III; Wang, J.; Moens, L.; Hensley, J. E. *Green Chem.* **2014**, 16, 454–490.
- 8 Nakagawa, Y.; Liu, S.; Tamura, M.; Tomishige, K. *ChemSusChem* **2015**, 8, 1114–1132.
- 9 Ng, L. Y.; Andiappan, V.; Chemmangattuvalappil, N. G.; Ng, D. K. S. *Ind. Eng. Chem. Res.* **2015**, 54, 5722–5735.
- 10 Paul, S.; Sarkar, B.; Bose, P. K. *Renew. Sus. Energy Rev.* **2015**, 48, 256–263.
- 11 Li, Q.; Zhang, Y.; Hu, G. *Bioresour. Technol.* **2015**, 191, 88–96.
- 12 Yang, Z.; Kumar, A.; Huhnke, R. L. *Renew. Sus. Energy Rev.* **2015**, 50, 859–870.
- 13 Badawi, M.; Cristol, S.; Paul, J.; Payen, E. *C. R. Chimie* **2009**, 12, 754-761.
- 14 Chiranjeevi, T.; Kumaran, G. M.; Gupta, J. K.; Dhar, G. M. *Pet. Sci. Technol.* **2008**, 26, 690-703.
- 15 Chiranjeevi, T.; Kumaran, G. M.; Gupta, J. K.; Dhar, G. M. *Thermochim. Acta* **2006**, 443, 87-92.
- 16 Chiranjeevi, T.; Kumaran, G. M.; Gupta, J. K.; Dhar, G. M. *Catal. Comm.* **2005**, 6, 101-106.
- 17 Furimsky, E. *Appl. Catal.* **1983**, 6, 159-164.
- 18 Pratt, K. C., Christoverson, V. *Fuel Process. Technol.* **1983**, 8, 43-51.

- 1  
2  
3  
4  
5  
6  
7  
8  
9  
10  
11  
12  
13  
14  
15  
16  
17  
18  
19  
20  
21  
22  
23  
24  
25  
26  
27  
28  
29  
30  
31  
32  
33  
34  
35  
36  
37  
38  
39  
40  
41  
42  
43  
44  
45  
46  
47  
48  
49  
50  
51  
52  
53  
54  
55  
56  
57  
58  
59  
60
- 
- 19 Furimsky, E. *Ind. Eng. Chem. Prod. Res. Dev.* **1983**, *22*, 31-34.
- 20 Mironenko, A. V.; Gilkey, M. J.; Panagiotopoulou, P.; Facas, G.; Vlachos, D. G.; Xu, B. *J. Phys. Chem. C* **2015**, *119*, 6075–85.
- 21 Chia, M.; Pagán-Torres, Y. J.; Hibbitts, D.; Tan, Q.; Pham, H. N.; Datye, A. K.; Neurock, M.; Davis, R. J.; Dumesic, J. A. *J. Am. Chem. Soc.* **2011**, *133*, 12675–12689.
- 22 Bradley, M. K.; Robinson, J.; Woodruff, D. P. *Surf. Sci.* **2010**, *604*, 920–925.
- 23 Horiuchi, C. M.; Medlin, J. W. *Langmuir* **2010**, *26*, 13320–13332.
- 24 Caldwell, T. E.; Land, D. P. *Polyhedron* **1997**, *16*, 3197–3211.
- 25 Bartók, M.; Szöllösi, G.; Apjok, J. *React. Kinet. Catal. Lett.* **1998**, *64*, 21–28.
- 26 Vannice, M. A. *Catal. Today* **1992**, *12*, 255-267.
- 27 Kreuzer, K.; Kramer, R. *J. Catal.* **1997**, *167*, 391-399.
- 28 Gennari, U.; Kramer, R.; Gruber, H. L. *Appl. Catal.* **1988**, *44*, 239-250.
- 29 Gennari, U.; Kramer, R.; Gruber, H. L. *Appl. Catal.* **1984**, *11*, 341-351.
- 30 Notheisz, F.; Bartok, M. *J. Catal.* **1981**, *71*, 331-336.
- 31 Bartok, M.; Notheisz, F. *J. Catal.* **1981**, *68*, 209-212.
- 32 Maity, S. K.; Rana, M. S.; Bej, S. K.; Ancheyta-Juarez, J.; Dhar, G. M.; Rao, T. S. R. P. *Catal. Lett.* **2001**, *72*, 115-119.
- 33 Rao, K. S. P.; Khajamasthan, S.; Muralidhar, G.; Chary, K. V. R.; Subrahmanyam, V. S. *J. Chem. Soc., Chem. Commun.*, **1988**, 375-376.
- 34 He, Z.; Wang, X. *Catal. Today*, **2014**, *240*, 220–228.
- 35 Bui P.; Cecilia, J. A.; Oyama, S. T.; Takagaki, A.; Infantes-Molina, A.; Zhao, H.; Li, D.; Rodríguez-Castellón, E.; Jiménez-López, A. *J. Catal.* **2012**, *294*, 184-198.
- 36 Cho, A.; Kim, H.; Iino, A.; Takagaki, A.; Oyama, S. T. *J. Catal.* **2014**, *318*, 151–161.
- 37 Iino, A.; Cho, A.; Takagaki, A.; Kikuchi, R.; Oyama, S. T. *J. Catal.* **2014**, *311*, 17-27.
- 38 Cho, A.; Shin, J.; Takagaki, A.; Kikuchi, R.; Oyama, S. T. *Top. Catal.* **2012**, *55*, 969-980.
- 39 Bowker, R. H.; Smith, M. C.; Pease, M. L.; Slenkamp, K. M.; Kovarik, L.; Bussell, M. E. *ACS Catal.* **2011**, *1*, 917–22.
- 40 Oyama, S. T.; Gott, T.; Zhao, H.; Lee, Y-K. *Catal. Today*, **2009**, *143*, 94–107.
- 41 Prins, R.; Bussell, M. E. *Catal. Lett.* **2012**, *142*, 1413–1436.
- 42 Kanda, Y.; Uemichi, Y. *J. Jap. Pet. Ins.* **2015**, *58*, 20-32.

- 1  
2  
3  
4  
5 43 Zhao, H. Y.; Li, D.; Bui, P.; Oyama, S. T. *Appl. Catal., A* **2011**, 391, 305-310.  
6  
7 44 Li, D.; Bui, P.; Zhao, H.Y.; Oyama, S. T.; Dou, T.; Shen, Z. H. *J. Catal.* **2012**, 290, 1-12.  
8  
9 45 Eigenman, H. K.; Golden, D. M.; Benson, S. W. *J. Phys. Chem.* **1973**, 77, 1687-1691.  
10  
11 46 Soundararajan, S.; Anantakrishnan, S. V. *Proc. Indian Acad. Sci., A* **1953**, 37, 578-583.  
12  
13 47 Weisz, P. B.; Prater, C. D. *Adv. Catal.* **1954**, 6, 143-196.  
14  
15 48 Vannice, M. A. *Kinetics of Catalytic Reactions*; Springer US, 2005, Chapter 4, pp 63-65.  
16  
17 49 Yuan, Q.; Ariga, H.; Asakura, K. *Top. Catal.* **2015**, 58, 194-200.  
18  
19 50 Oyama S. T.; Gott T.; Asakura K.; Takakusagi S.; Miyazaki K.; Koike, Y.; Bando K. K. *J.*  
20  
21 *Catal.* **2009**, 268, 209-222.  
22  
23 51 Bando, K. K.; Wada, T.; Miyamoto, T.; Miyazaki, K.; Takakusagi, S.; Koike, Y.; Inada,  
24  
25 Y.; Nomura, M.; Yamaguchi, A.; Gott, T.; Oyama, S. T.; Asakura, K. *J. Catal.* **2012**,  
26  
27 286,165-171.  
28  
29 52 Wada, T.; Bando, K. K.; Miyamoto, T.; Takakusagi, S.; Oyama, S. T.; Asakura, K. *J.*  
30  
31 *Synchrotron Radiat.* **2012**, 19, 205-209.  
32  
33 53 Badaria, C. A.; Lónyi, F., Drotára, E.; Kaszonyi, A.; Valyona, J. J. *Appl. Catal. B: Env.*  
34  
35 2015,164, 45-60.  
36  
37 54 Zhao, H.Y.; Oyama, S. T.; Freund, H-J.; Wlodarczyk, R.; Sierka, M. *Appl. Catal., B* **2015**,  
38  
39 164, 204-216.  
40  
41 55 Nelson, A. E.; Sun, M.; Junaid, A. S. M. *J. Catal.* **2006**, 241, 180–188.  
42  
43 56 Oyama, S. T.; Zhao, H.; Freund H-J.; Asakura, K.; Wlodarczyk, R.; Sierka, M. *J. Catal.*  
44  
45 **2012**, 285, 1–5.  
46  
47 57 Hernandez, A. B.; Ariga, H.; Takakusagi, S.; Kinoshita, K.; Suzuki, S.; Otani, S.; Oyama,  
48  
49 S. T.; Asakura, K. *Chem. Phys. Lett.* **2011**, 513, 48-52.  
50  
51 58 Ariga, H, Kawashima, M.; Takakusagi, S.; Asakura, K. *Chem. Lett.* **2013**, 42, 1481-1483.  
52  
53 59 Guo, D.; Nakagawa, Y.; Ariga, H.; Suzuki, S.; Kinoshita, K.; Miyamoto, T.; Takakusagi,  
54  
55 S.; Asakura, K.; Otani, S.; Oyama, S. T. *Surf. Sci.* **2010**, 604, 1347–1352.  
56  
57 60 Moon, J. S.; Kim, E. G.; Lee, Y-K. *J. Catal.* **2014**, 311, 144-152.  
58  
59 61 Suzuki, S.; Moula, G. M.; Miyamoto, T.; Nakagawa, Y.; Kinoshita, K.; Asakura, K.;  
60  
Oyama, S. T.; Otani, S. *J. Nanosci. Nanotechnol.* **2009**, 9, 195-201.

- 
- 1  
2  
3  
4  
5 62 Liu, P.; Rodriguez, J. A.; Asakura, T.; Gomes, J.; Nakamura, K. *J. Phys. Chem. B* 2005,  
6 109, 4575-4583.  
7  
8 63 Ariga, H.; Kawashima, M.; Takakusagi, S.; Asakura, K. *Chem. Lett.* 2013, 42, 1481-1483.  
9  
10 64 Lee, Y.-K.; Oyama, S.T. *J. Catal.* 2006, 239, 376-389.  
11  
12  
13  
14  
15  
16  
17  
18  
19  
20  
21  
22  
23  
24  
25  
26  
27  
28  
29  
30  
31  
32  
33  
34  
35  
36  
37  
38  
39  
40  
41  
42  
43  
44  
45  
46  
47  
48  
49  
50  
51  
52  
53  
54  
55  
56  
57  
58  
59  
60

